JACS
JOURNAL OF THE AMERICAN CHEMICAL SOCIETY

Article

pubs.acs.org/JACS

Noble-Metal-Free Electrocatalysts with Enhanced ORR Performance by Task-Specific Functionalization of Carbon using Ionic Liquid Precursor Systems

Nastaran Ranjbar Sahraie,[†] Jens Peter Paraknowitsch,*[,‡] Caren Göbel,[‡] Arne Thomas,[‡] and Peter Strasser*[,†]

[†]The Electrochemical Energy, Catalysis, and Materials Science Laboratory, Department of Chemistry, Chemical Engineering Division, Technical University Berlin, Straße des 17. Juni 124, 10623 Berlin, Germany

[‡]Department of Chemistry, Division of Functional Materials, Technical University Berlin, Hardenbergstraße 40, 10623 Berlin, Germany

Supporting Information

ABSTRACT: The synthesis and characterization of functionalized carbon using variable doping profiles are presented. The hybrids were obtained from nitrile-functionalized ionic precursors and a ferric chloride mediator. This way, novel nitrogen doped and nitrogen−sulfur, nitrogen−phosphorus, and nitrogen−boron codoped carbon hybrids with a morphology containing microporous nanometer-sized particles were obtained. As-prepared heteroatom doped carbons exhibited superior electrocatalytic activity toward the oxygen reduction reaction (ORR) in alkaline and acid electrolytes. In particular, both the heteroatom type and iron were found to play crucial roles in improving the catalytic activity of functionalized carbon. It is worth noting that sulfur−nitrogen codoped functionalized materials synthesized in the presence of ferric chloride showed higher activity and stability in comparison to those of the commercial state-of-the-art Pt catalyst in alkaline electrolyte. Moreover, in acid electrolyte, sulfur−nitrogen codoped catalyst rivaled the activity of Pt with a stability outperforming that of Pt. Our X-ray photoelectron spectroscopy (XPS) investigation revealed a distinctive atomic structure in nitrogen−sulfur codoped material in comparison to other codoped catalysts, most likely explaining its superior electrocatalytic activity. This work presents a novel toolbox for designing advanced carbon hybrids with variable heteroatom doping profiles which presents tunable and enhanced ORR performance.

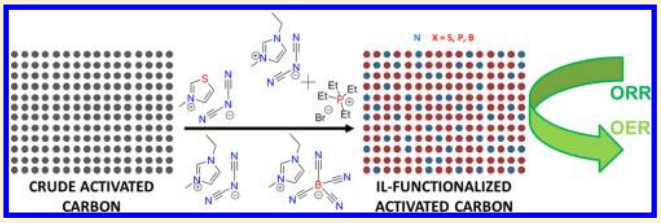

INTRODUCTION

Proton exchange membrane fuel cells (PEMFCs) as well as alkaline liquid and alkaline membrane fuel cells (AFCs) fed with pure hydrogen or hydrogen-rich gas fuels from renewable sources are appealing substitutes for conventional power generator devices. Currently, Pt and Pt alloys supported on carbon are used in cathodes and anodes of PEMFCs, while silver on carbon is often used in AFC cathodes. High loadings of Pt at the cathode are necessary to surmount the intrinsically sluggish kinetics of ORR. These high loadings mean high cost, which is a substantial hurdle for widespread mass production of affordable PEMFCs. Hence, there is a prerequisite for increasing the Pt mass specific activity of the catalyst by lowering the Pt content through alloying with other non noble metals. However, in the long term, complete substitution of precious metals with non-noble-metal catalysts (NNMCs) with high ORR activity and stability remains a major scientific and technical target. To reach this goal, a large number of nitrogen-, metal-, and carbon-derived catalysts have been explored, originally on the basis of a bioinspired molecular metal−porphyrin concept with well-defined nitrogen-coordinated metal ion centers.[1] The very first non-noble-metal catalysts showed very low activity in comparison to Pt-based cathode materials under PEMFC conditions. However, over the past three decades, outstanding progress has been made in terms of their performance / stability. Recently, advanced characterization techniques enabled us to perform fundamental studies and mechanistic investigations on non-noble-metal catalysts. Advances in the synthesis of NNMCs made the replacement of Pt with earth-abundant metal-based catalysts an accessible reality. However, regardless of all these achievements, the nature of the active site for this class of materials is still under discussion. Accordingly, in the future, the research should focus on investigatng active sites as well as increasing the density of these sites either by optimizing the nitrogen doping level or optimizing the morphology of the catalyst. More recent works on nonprecious ORR catalysts have focused on material-like concepts where nitrogen−metal coordination is believed to be embedded in a solid-state carbon structure. Thus, the catalyst precursors (carbon, nitrogen, and metal sources) play particularly significant roles in catalytic performance. The

Received: June 30, 2014
Published: September 15, 2014

   dx.doi.org/10.1021/ja506553r | J. Am. Chem. Soc. 2014, 136, 14486−14497

crucial role of the metal in ORR activity of non-noble-metal catalysts has been proven in the literature, in particular in acid electrolyte.[2−6] Traditionally, wet impregnation of high-surface-area carbons with nitrogen and iron precursors followed by high-temperature pyrolysis (800−1000 °C) was one of the first synthetic strategies used to synthesize low-cost NNMCs. These materials successfully replaced expensive macromolecules.[7−11] In 2009, Dodelet et al. introduced a novel material called a pore filler by using a ball-milling strategy which successfully replaced the wet impregnation synthesis strategy.[11]

It is assumed that the type of coordinating heteroatom can affect the structural and electronic environment of the metal ion and thus may be used to tune the catalytic activity and stability.[12] All these calls for a more in-depth investigation of novel nonprecious ORR catalysts are based on new precursor combinations and alternative heteroatoms. Recently, heteroatoms other than nitrogen, such as sulfur, phosphorus, and (in particular) boron, were used for (co)doping of carbon for the preparation of ORR catalysts.[13−18] However, all previously reported materials showed ORR performances in alkaline and acid media lower than that of the Pt/C reference catalyst.[19,20] This report sheds new light on a novel family of ionic liquid derived heteroatom doped materials and reveals their true potential as candidates for synthesis of highly active ORR catalysts.

Ionic liquids (ILs) have been investigated intensely since their very first discovery in 1914, when a low melting point of ethylammonium nitrate of only 12 °C was observed.[21] Typically, sterically demanding and asymmetric ions are used which hinder ordered packing of ions, resulting in low melting points below 100 °C. The range of synthetically accessible ILs is tremendously wide, and due to the possibility of combining chemically versatile anions and cations, the property profiles can be tuned widely. Therefore, ILs have found their way into different fields of applications, e.g.—among others—as solvents,[22−25] as electrolytes in batteries or capacitors, in catalytic applications,[25−29] or in the synthesis of materials.[30−36]

One class of ILs which is widely characterized consists of nitrogen-containing cations and nitrile functional groups: e.g., in dicyanamide anions. It is worth noting that they carbonize upon thermal treatment, which results in nitrogen-doped carbon materials with excellent electric conductivities and thermal stabilities.[31,37−41] Later, the precursors were modified to allow for the incorporation of additional heteroatoms into the carbon materials. The first works in this context have been presented regarding boron and nitrogen codoped carbons, while the boron was introduced by using tetracyanoborate anion containing ILs.[42,43] By the use of thiazolium cations, the coincorporation of sulfur atoms in addition to nitrogen became possible.[44] Recently, ethylmethylimidazolium isothiocyanate has been reported to act suitably as a precursor for S/N codoped carbon materials.[45] Moreover, phosphorus and nitrogen codoped carbon materials have been successfully prepared.[46]

Most of the prior work on IL precursors for the formation of doped carbon materials has focused on their direct carbonization at high temperatures (800−1000 °C).[37−40,42−46] Despite the interesting properties and excellent processibility of these liquid precursors, the direct use of IL precursors for carbonization is not economical due to the high cost as well as low carbonization yield (around 20 wt % on the basis of TGA studies).[39,40] Therefore, only a few studies have reported their application for electrochemical catalysis, either as a host for electrocatalytically active platinum nanoparticles[47] or as electrocatalysts themselves.[48,49] Nevertheless, the different heteroatom doping profiles that are so easily accessible and adjustable can potentially represent a synthetic toolbox predetermined for application as ORR catalysts: nitrogen tunes the electronic structure of carbons in a way that facilitates the enhanced interaction with oxygen and its subsequent catalytic conversion.[50] Similarly, the electronic modifications caused by boron doping have shown benefits for electrochemical oxygen conversion.[51,52] Phosphorus and sulfur, in contrast, do not have a significant influence on the electronic structure of the carbons, but they can—due to their size—enhance carbonaceous structure polarizability. Accordingly, the applicability of the doped materials as electrocatalysts was proven in different studies.[53,54] Multiple heteroatom doped carbons appear to be highly interesting candidates for ORR catalysts.[18] Hence, finding more economic pathways toward the application of IL-derived carbon materials is highly desirable. In order to develop practical uses for these IL-derived carbon materials, their application should be oriented toward hybrids with commercially available bulk carbons. Accordingly, creating a thin coating layer in a composite-like material with a thermally stable carbon backbone instead of using the mere materials is a solution. This concept is relatively new in the field of IL-derived carbons. In this case, a crude carbon could be finely modified by a minimal functionalization with ILs. It has been shown that this functionalization enhances the long-term stability of loaded platinum nanoparticles during their electrochemical performance, significantly in comparison to particles loaded on crude carbon nanotubes.[55] It could thus be shown that it is possible to transfer the beneficial properties of the IL carbon to cheaper bulk carbon backbones by simple hybrid formation, avoiding the consumption of large amounts of IL. However, the previous reported works on the application of ionic liquids for doping of commercial carbon were limited to single doping (nitrogen doped), which showed low activity and in particular low selectivity toward ORR.

In this work, we explore the synthesis and ORR electrocatalysis of a novel family of functionalized carbon with different heteroatom-doping profiles in alkaline and acid electrolytes. We prepared nitrogen doped and nitrogen−sulfur, nitrogen−phosphorus, and nitrogen−boron codoped carbon hybrids. As-prepared heteroatom doped carbons exhibited a high electrocatalytic activity and long stability toward the oxygen reduction reaction in the presence of metal (iron). We show that both the heteroatom type and the metal play significant roles in improving the catalytic activity of the final carbon material. Obviously, the role of nitrogen in changing the electronic structure of pure carbon not only can be successfully transferred to other heteroatoms, such as sulfur, phosphorus, and boron, but also can be improved, as seen in the nitrogen−sulfur sample. In this work, by the selection of an appropriate codoping agent—sulfur—the activity can be greater that of Pt catalyst. Accordingly, a sulfur-nitrogen codoped sample—the best performing catalyst—synthesized in the presence of ferric chloride showed superior activity and stability in comparison to that of pure carbon as well as a commercial state of the art Pt catalyst in alkaline electrolyte. In acid electrolyte, sulfur−nitrogen codoped catalyst competed with the activity of Pt with a stability outperforming that of Pt. X-ray photoelectron spectroscopy (XPS) was applied to probe the atomic structure of the doped materials. The effect of both the heteroatom type and the metal on the electrocatalytic activity of carbon is

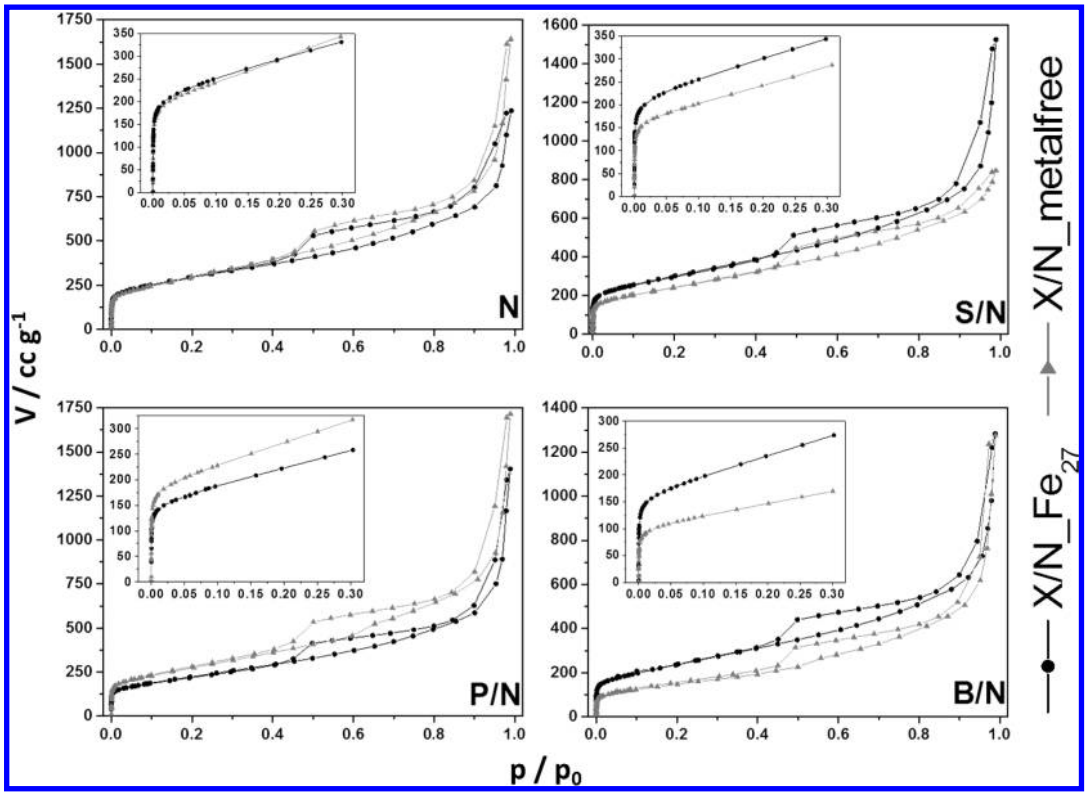

Figure 1. Nitrogen sorption isotherms of differently codoped materials. All materials were synthesized using Ketjenblack carbon and different single- and double-heteroatom ionic liquid precursors (N, EMIM-dca; S/N, THIA-dca; P/N, EMIM-dca + TEPBr; B/N, EMIM-tcb; Figure S1, Supporting Information). X/N_metalfree (triangles) refers to metal-free samples, while X/N_Fe_{27} (circles) refers to samples with a nominal 27 wt % of Fe. X in all cases refers to the respective codopant S, P, or B. Insets show magnification of the low-pressure region. A comparison to pure Ketjenblack is provided in Figure S2 (Supporting Information).

discussed here. In particular, the structure of the nitrogen−sulfur codoped material in comparison to those of other codoped catalyst was studied to explain the former's superior electrocatalytic activity. To the best of our knowledge, this is the first time that numerous ionic liquid precursors have been systematically used for codoping of commercial carbons. We could show that simultaneous doping of carbon with two heteroatoms has a determining role in the catalytic activity of the final doped material.

■ EXPERIMENTAL SECTION

Sample Preparation. Carbon nanoparticles were functionalized using ionic precursor systems containing cyano functional groups. Therefore, carbon black was dispersed in an aqueous solution of the chosen precursor system shown in Figure S1 (Supporting Information). Typically, 550 mg of the IL precursor was dissolved in 100 mL of water. All samples were additionally prepared using $FeCl_3$ as a mediator, dissolving it into the reaction mixture in a concentration aiming at 27 wt % of iron respective to the mass of carbon used. After equilibration with vigorous stirring of the mixtures, their volumes were reduced and thermal treatment under inert gas at 900 °C was performed. The metal-free samples were tested without any further treatment, while metal-containing samples were treated with acid (sulfuric acid; c = 2 mol L^{-1}) to leach out as much residual metal as possible and subsequently annealed at 900 °C for a second time. By application of this method, a number of carbon systems were functionalized with different heteroatom doping profiles. Four ionic liquid based single- and double-heteroatom precursors (N, S/N, P/N, and B/N; see Figure 1) were used to prepare four heteroatom doped Fe-containing materials as well as four analogous heteroatom doped metal-free samples. Accordingly, samples are assigned as X/N_Fe_x, in which X is the second respective heteroatom and x is the Fe nominal concentration (before acid leaching) respective to the carbon in the synthetic mixture. The metal-free materials will henceforth be denoted only by their heteroatom doping ("N", "S/N", "P/N", and "B/N"), while the Fe-containing catalysts will carry the extension "_Fe_x" where x denotes the metal weight content in the synthetic mixture. Additionally, more synthetic parameters were varied upon the formation of materials. These variations that were applied only on the N-doped materials include (i) different metal contents in the synthesis mixture (27, 10, and 5 wt % samples assigned as N_Fe_{27}, N_Fe_{10}, and N_Fe_5, respectively) and (ii) a second acid leaching step after the second thermal treatment, followed by a third thermal treatment (referred to as N_Fe_{27}-2, N_Fe_{10}-2, and N_Fe_5-2). More detailed synthetic protocols are described in the Supporting Information.

■ CHARACTERIZATION OF THE MATERIALS

The catalyst materials were analyzed regarding their microporosities, nanomorphologies, and heteroatom contents.

Porosity and Sorption Behavior. The nitrogen sorption isotherms of all materials have been measured and are illustrated in Figure 1. In comparison to that of the pure carbon (Figure S2, Supporting Information), the isotherms are not significantly altered by the heteroatom and metal functionalization. In all cases, the isotherms can be essentially classified as type I, proving that all materials are microporous.

Only the relatively high slopes at the highest relative pressures represent a deviation from an ideal type I isotherm in the as-synthesized catalysts. This indicates the contribution of external surface area to the isotherms, which can be easily explained by the particular structure of the carbon nanoparticles. These particles seem to aggregate and thereby form

dx.doi.org/10.1021/ja506553r | J. Am. Chem. Soc. 2014, 136, 14486−14497

interparticle porosities, which is derived from the presence of very broad hysteresis loops (type H3).[56] This interparticularly formed porosity is more pronounced for the functionalized carbon samples. The BET surface areas[57] of the samples decrease slightly in comparison to crude Ketjenblack but are still significantly high with values between 800 and 1100 $m^2\ g^{-1}$ (summary in Table 1). Only the metal-free B/N sample showed a somewhat reduced surface area, likely caused by an increase of partial pore blocking. Still, the observed surface area is sufficiently high, while the pronounced slope of the isotherm in the low-pressure region of the metal-free B/N sample is evidencing a significant amount of microporosity.

Table 1. BET Surface Areas ($m^2\ g^{-1}$) of Differently Functionalized Carbons, either without the Use of Metals or with $FeCl_3$ during Synthesis with 27 wt % Concentration of Iron Respective to Carbon with Performance of the First Acid Leaching/Second Pyrolysis Step for Iron Residue Removal and Recovery of Catalyst Surface, Respectively

sample	N	S/N	P/N	B/N
metal-free sample	1072	881	990	530
Fe_{27} sample	1043	1079	806	855

Morphological Analysis of the Heteroatom-Doped Hybrids. In order to investigate the homogeneity of the catalyst samples and exclude the presence of bulky heteroatom-doped carbon residues in the interparticular space of the carbon, transmission electron microscopy (TEM) was applied. Our TEM study started with the hypothesis that a homogeneous morphology would imply a successful functionalization of carbon. The observed morphology of all catalyst materials consisted of partially cross-linked particles in the size range of 10−50 nm and was very similar to that of the pure and untreated carbon precursor (see Figures S3 and S4, Supporting Information). Indeed, there was no identification of any interparticular bulk carbon residues, which prompted the conclusion of a successful functionalization of carbon. We therefore further conclude that the interaction between the carbon and the ionic precursors suppressed the isolated carbonization of precursor molecules into heterogeneous carbon/carbonized precursor composites in favor of homogeneous heteroatom-functionalized carbon hybrids. Further evidence came from scanning electron micrographs (SEM) that were obtained for the carbon reference and as-synthesized S/N_Fe_{27} catalyst. Again, these SEM micrographs (see Figure S5, Supporting Information) reconfirmed the identical morphology and support the conclusion of a new hybrid formed of carbon and IL precursors.

Elemental Analysis. To address the extent of heteroatom doping, we performed elemental analysis by either elemental flash combustion analysis (EA) or inductively coupled plasma-optical emission spectroscopy (ICP-OES). The results are presented in Table S1 (Supporting Information). All as-prepared materials exhibited the targeted heteroatom doping profile. In particular, the influence of iron chloride during the synthesis on the extent of heteroatom doping is noteworthy. The metal is mediating the chemical reaction toward the doped carbon systems in a way that leads to a reduced incorporation of heteroatoms, except for nitrogen in the P/N material. Additionally, the amount of nitrogen is extraordinarily high for the metal-free B/N sample, which is due to the higher amount of polymerizable nitrile groups in the anion of the starting ionic liquid precursor. The mediating effect of the metal is yet also decreasing the heteroatom contents in the B/N_Fe_{27} sample. In the X/N_Fe_{27} samples, traces of iron are found that remained as residues after the acid leaching procedure, in amounts of ∼1.5 wt % for all samples.

Wide-Angle X-ray Powder Diffraction Analysis of the Heteroatom-Doped Hybrids. Wide-angle X-ray scattering (WAXS) offered further insight into the structural long-range order of the as-synthesized samples (Figure 2).

The profiles showed characteristic reflections of crystalline iron carbide in the materials which were synthesized with $FeCl_3$. All X/N_Fe_{27} catalyst materials, except one, display clear iron residues in form of Fe_3C.[58,59] Interestingly, this is not the case for the P/N_Fe_{27} sample, although the iron content of this material is in the same range in comparison to other samples (see Table S1, Supporting Information). From the absence of any Fe-related crystalline phase, we conclude that, in P/N_Fe_{27}, iron must be present in an amorphous and different chemical state than in the other samples. Apart from the iron carbide fingerprints, the WAXS patterns exhibited the typical shape of condensed carbon materials with a limited degree of graphitization represented by the broadened reflexes in all the samples, regardless of the presence of the metal. Peak widths of

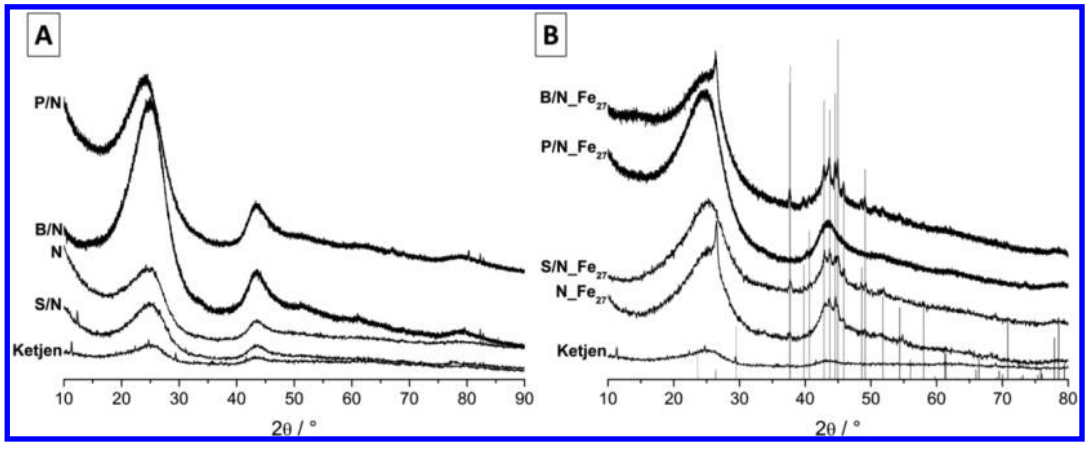

Figure 2. WAXS patterns of the heteroatom doped metal-free and metal-containing materials: (A) Ketjenblack carbon reference and metal-free heteroatom-doped samples; (B) Ketjenblack carbon reference and metal-containing heteroatom doped samples. The vertical diffraction line patterns in panel B are denoted at base-derived Fe_3C diffraction lines.[58,59]

dx.doi.org/10.1021/ja506553r | J. Am. Chem. Soc. 2014, 136, 14486−14497

carbon and catalysts suggest that, due to the thermal treatment, the graphitization increased slightly. Interestingly, there is no evidence for a significant influence of iron in the X/N_Fe_{27} materials on the overall degree of graphitization of the carbon hybrid materials.

X-ray Photoelectron Spectroscopy of Heteroatom-Doped Hybrids. The detailed chemical environments of the heteroatoms in the near-surface region of the catalyst materials were investigated using X-ray photoelectron spectroscopy (XPS). The entire set of survey spectra (Figure S6) and their detailed discussion can be found in the Supporting Information. These survey spectra confirm the presence of carbon, nitrogen, and the respective codopants in all catalyst materials. Surprisingly, iron could not be detected in the near-surface region of any X/N_Fe_{27} samples, although its presence was confirmed by both ICP-OES and WAXS measurements. As XPS is a highly surface sensitive method, we conclude that the iron carbide or other iron residual species must be buried inside the bulk of carbon particles covered with a metal-free overlayer with nanometer scale thickness. Subsequently, detailed scans of the different core levels (C1s, N1s, S2p, P2p, and B1s) were analyzed as follows.

Carbon Core Level XPS Analysis. All C1s core level regions (see Figure S7, Supporting Information) were very similar, implying that the hybrid materials are close in their chemical environment of carbon. The shapes of the different core level spectra are asymmetrical and show a broad satellite at higher values of binding energy between ∼287 and ∼294 eV. A satellite feature in this region is typical for graphitic carbon binding situations and is caused by the delocalized π-electron system. This observation is in agreement with the WAXS patterns, corroborating a slight increase of the graphitization during the heat treatment of the materials. Furthermore, in this higher binding energy region, oxidized carbon species appear, which could be the reason for the observation of these satellite peaks.[60,61] The presence of these peaks is typical for carbon materials handled in a normal air atmosphere. Nevertheless, the two—by far more dominant—contributions to the spectra at ∼284.3 eV and at around 285 eV are of higher significance. At ∼284.3 eV carbon atoms neighboring other carbon atoms in a sp^2 binding environment are represented, while at the higher binding energies, carbon atoms are bound to more electronegative binding partners. This can be ascribed to the presence of nitrogen-bound carbon atoms. Furthermore, the other heteroatoms in different carbon structures can likewise contribute to such a shift in binding energy.[60−62] In summary, the carbon core spectra reveal heteroatom-functionalized carbon hybrid materials in which the heteroatoms are anchored within a carbon backbone with a graphitic microstructure. Additionally, S/N_Fe_{27} and B/N_Fe_{27} showed some contributions at lower binding energies of ∼283 eV, which are typical for carbon atoms bound in carbide-like chemical environments. Therefore, the seeming conflict of the iron absence in XPS is actually consistent with the presence of crystalline iron carbide residues seen in the XRD patterns. This observation can be considered as a hint of low amounts of metal residues in the samples in form of iron carbide moieties.[63] However, in agreement with the WAXS patterns, this feature was not observed for P/N_Fe_{27} samples.

Nitrogen Core Level XPS Analysis. While the peaks around 286 eV showed that carbon is bound to heteroatoms, especially the more electronegative ones, it is of further interest to investigate the respective core level spectra of the heteroatoms in the materials with their manifold doping profiles. A closer look at the N1s core level spectra is provided in Figure 3. It should be mentioned that peak fitting was not applied for N_Fe_{27} and S/N_Fe_{27} samples due to the signal-to-noise ratio of the obtained spectra. From a rather qualitative analysis of corresponding intensities, it can nevertheless be concluded that the binding energies are similar to those observed for the samples on which a detailed peak fitting was scientifically permitted.

All N1s core level spectra exhibit an asymmetrical shape and thus a broadened contribution at high binding energy values of >404 eV. This feature can be, on the one hand, attributed to oxidized nitrogen species on the materials' surfaces.[61,64] On the other hand, the high binding-energy tail can be interpreted as a satellite feature caused by π electrons of nitrogen atoms bound in an aromatic chemical environment. This satellite peak reveals the chemical state of the nitrogen atoms in differently functionalized carbon hybrids as being firmly incorporated into the carbon backbones. In this case, confirmation stems from the presence of the two dominant peak contributions, which appear at binding energies between 398.2 and 398.7 eV and at binding energies between ∼400 and ∼401 eV in all N1s spectra.[61,65] The former spectral feature corresponds to pyridinic or pyrrolic nitrogen, representing nitrogen atoms bound at the edges of graphite layers. The latter corresponds to the graphitic nitrogen atoms, referring to nitrogen atoms truly replacing carbon atoms in graphene-sheet binding environments with the excess electron delocalized in the π system (sp^2 hybridized).[61,64−66] Our findings are consistent with the notion that nitrogen is firmly incorporated into the carbon backbone, which is the preferred situation for the formation of catalytically active centers in heteroatom-doped carbon hybrid materials. Analysis of the influence of the iron chloride mediator on the nature or extent of any of the two different major nitrogen bonding states revealed no such effect. Hence, as the use of $FeCl_3$ did have a significant impact on the resulting electrocatalytic ORR performance (see below), we conclude that the chemical state of nitrogen is less of a controlling factor for catalytic performance than previously thought.

Heteroatom Core Level XPS Analysis. In addition to nitrogen, the other heteroatoms in the codoped hybrids were analyzed using the core level spectra of the S2p, P2p, and B1s orbitals. The spectra, including their deconvoluted peaks, are depicted in Figure 4.

A closer look at the S2p core level spectrum reveals that both S/N_metalfree and S/N_Fe_{27} exhibit identical chemical environments for the sulfur atoms in the materials. The splitting into two peaks with maxima at ∼163.6 and ∼164.8 eV represents the spin−orbit related peak splitting of 1.18 eV for the S2p core level.[60] Therefore, we can conclude that most likely the sulfur atoms are bound in one predominant chemical state. Binding energies of ∼163.6 eV for the S2p 3/2 peak can refer to aromatic, thiophene-like binding environments, sulfur bridges between aromatic carbon features, or sulfur atoms building up double bonds to carbon.[67,68] The binding energies of sulfur atoms in these various chemical states are close and are hard to distinguish. However, they all represent sulfur that is firmly bound into a carbonaceous material, evidencing a successful incorporation of the sulfur. Furthermore, in studies on sulfur-substituted carbon nitride, very similar chemical binding energies were reported, suggesting S−C−N binding sites (caused by the replacement of nitrogen atoms in triazine

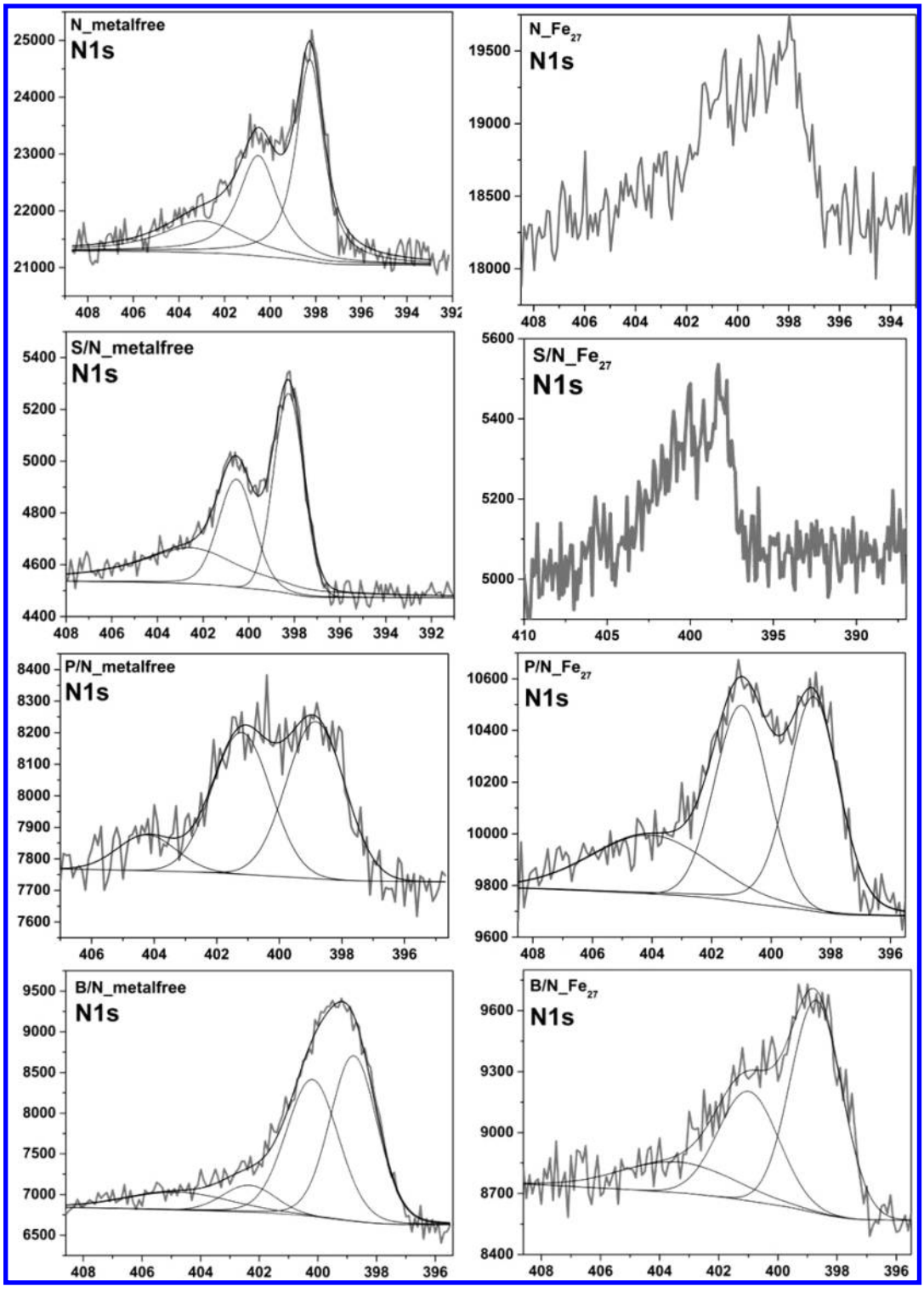

Figure 3. N1s core level XPS spectra of all X/N_metalfree and X/N_Fe_{27} materials. X in the sample assignation refers to the respective codopant applied in the synthesis, depending on the ionic precursor used. Fe_{27} refers to the use of $FeCl_3$ in the synthetic mixture (nominal 27 wt % of Fe with respect to Ketjenblack). *x* axes are BE values in units of eV; *y* axes are counts/s.

units by sulfur),[69] corroborating a successful codoping of sulfur and nitrogen into the hybrid electrocatalysts.

Similarly, phosphorus was analyzed according to the P2p core level spectra. Although the amount of phosphorus varies largely between P/N_metalfree and P/N_Fe_{27}, the chemical environments of phosphorus are basically identical (Figure 4C,D). Accordingly, two peak contributions appear in the deconvoluted spectra, due to the spin−orbit-related splitting of P2p. The P2p 3/2 peak at 133.02 eV (P/N_Fe_{27}) or 133.09 eV (P/N_metalfree) most probably represents phosphorus atoms directly bound to the nitrogen.[70,71] Such a phosphazene-like binding environment could not be clearly detected for nitrogen in the N 1s core level spectra, which is most likely due to the very similar binding energy in comparison to graphitic

dx.doi.org/10.1021/ja506553r | J. Am. Chem. Soc. 2014, 136, 14486−14497

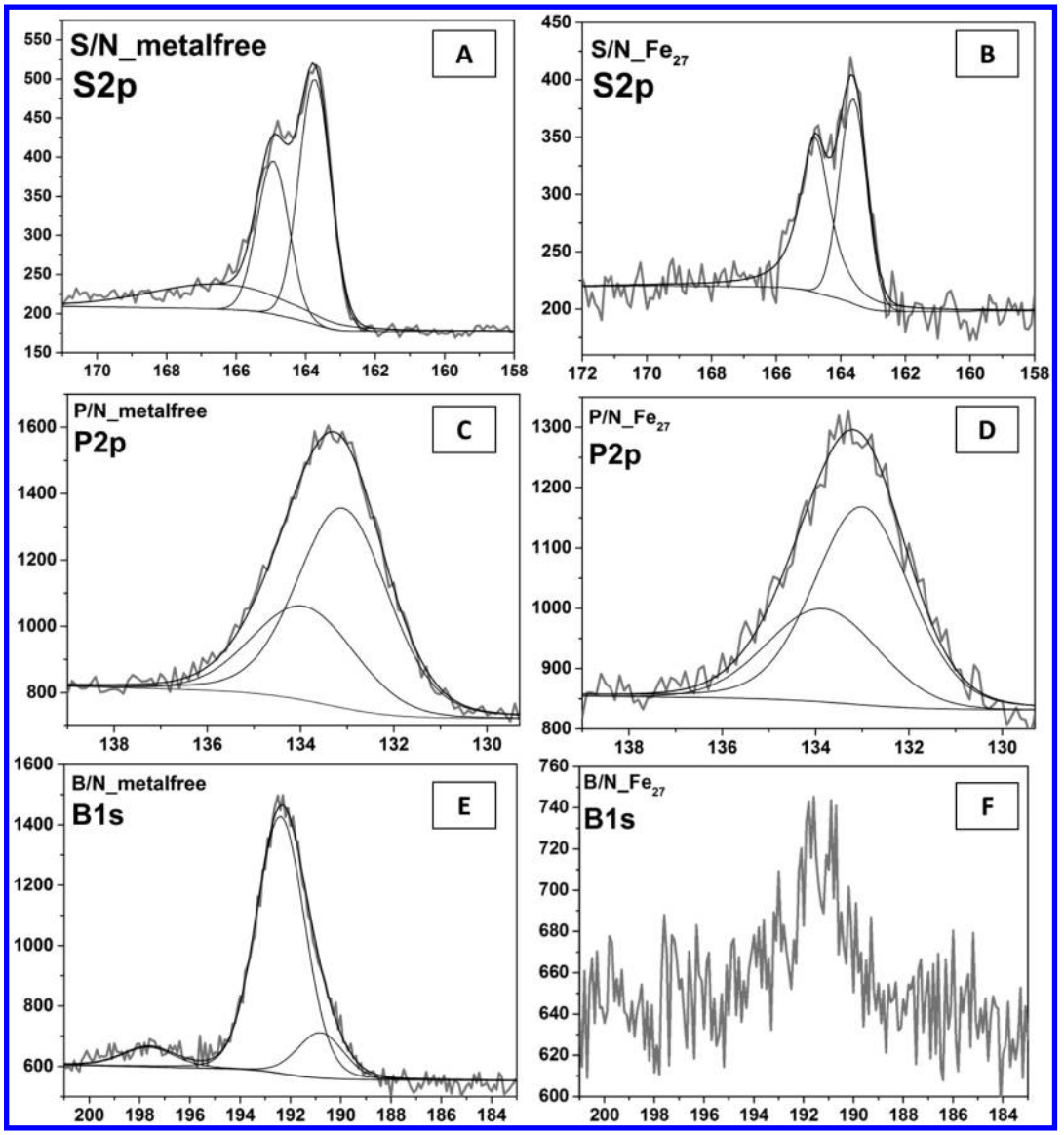

Figure 4. XPS core level spectra: (A, B) S2p for S/N materials; (C, D) P2p for P/N materials; (E, F) B1s for B/N materials. X in the sample assignation refers to the respective codopant in the material, depending on the ionic precursor used. Fe_{27} refers to the use of $FeCl_3$ in the synthetic mixture (27 wt % of Fe with respect to Ketjenblack. *x* axes are BE values in units of eV; *y* axes are in units of counts/s.

nitrogen.[72] Other chemical states to which a binding energy of ~133 eV may refer are quaternary alkyl phosphonium sites,[71] which is more unlikely considering the high synthesis temperature.

Due to the relatively low amount of boron in the B/N_Fe_{27} sample, the respective B1s core level spectrum (lower panel of Figure 4) is very noisy. In this case, the signal-to-noise ratio does not allow for a detailed peak fitting. In contrast, for the B/N_metalfree material, due to the much higher amount of boron, the B1s core level scan allows for a more explicit evaluation of the spectrum. Here, two dominant contributions appear at ~192.4 eV and—with less intensity—at ~190.9 eV. These values do not refer to the boron atoms exclusively bound to carbon, as boron carbide related structures exhibit smaller values for the binding energies at <189 eV.[73] These binding energies rather refer to boron atoms directly neighboring nitrogen atoms, as similar binding energies have been reported for boron nitride materials.[74] The very broad and weak contribution at higher binding energy values may be either a hint of the incorporation of the boron atoms into a graphite-like system or refer to oxygenated boron species at the surface of the material.

We conclude from XPS measurements that the hybrid catalyst materials are carbon materials with a graphite-related structure with the heteroatoms firmly bound and incorporated within these carbon backbones. Regarding the as-synthesized codoped materials, a significant structural difference between the S/N-functionalized and the P/N- and B/N-functionalized materials was observed: While for P/N and B/N dissimilar heteroatoms are largely in the atomic neighborhood with each other with direct bonds for P−N and B−N, the sulfur and nitrogen atoms in the S/N codoped materials seem to be doped in a spatially separated way. No proof for direct bonds between S and N were found. This crucial difference will turn out to correlate with differences in the electrocatalytic performance of the materials.

Effects of Fe Metal Loading. We studied the correlation between the initial Fe content in the synthesis mixture and the

dx.doi.org/10.1021/ja506553r | J. Am. Chem. Soc. 2014, 136, 14486−14497

corresponding residual content in the final "N_Fe$_x$" hybrid catalyst of Fe, carbon, hydrogen, and nitrogen and the correlation with its ORR activity. Actual elemental compositions of the "N_Fe$_x$" samples, where x denotes the initial Fe wt %, are summarized in Table S3 (Supporting Information). The data show that a decrease in initial metal content leaves the nitrogen content essentially constant, while the amount of residual iron follows the initial Fe content. Additional leaching/annealing steps reduce the residual Fe content significantly and the nitrogen content slightly. Since graphene sheet-incorporated nitrogen atoms are likely not eliminated by the additional sample treatment, this decrease is likely explained by a more efficient removal of oxidized nitrogen species at the surfaces of the materials. The decreased residual iron is also visible in WAXS patterns of the respective samples (compare parts A and B of Figure 5): in both cases, the intensities of the Fe carbide related reflexes decrease and almost disappear at the lowest applied ferric chloride concentrations.

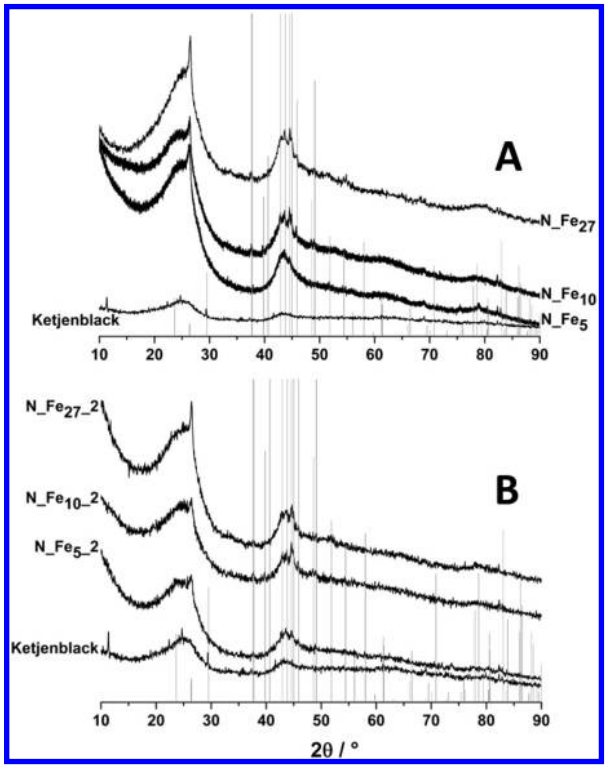

Figure 5. WAXS patterns for N-doped samples with modified synthetic parameters: (A) variation of ferric chloride nominal amount in the synthesis mixture; (B) second acid leaching and third thermal treatment. y axes are in arbitrary units.

ELECTROCHEMICAL ACTIVITY AND STABILITY OF HETEROATOM DOPED HYBRID CATALYSTS

Optimizing Fe Content. The catalytic activity of the heteroatom-doped hybrid catalysts was probed using linear sweep voltammetry (LSV) in 0.1 M KOH and 0.1 M $HClO_4$ electrolytes. For the family of "N_Fe$_x$" catalysts, the influence of the nominal metal loading ranging from 5 to 27 wt % on the oxygen reduction reaction activity under alkaline conditions is displayed in Figure 6. Metal-free N-doped carbon catalysts ("N_metalfree") and pure Pt serve as references. The greater catalytic activity of the hybrid systems "N_Fe$_5$" and "N_Fe$_{27}$" over that of the metal-free hybrid is obvious, as reflected in a

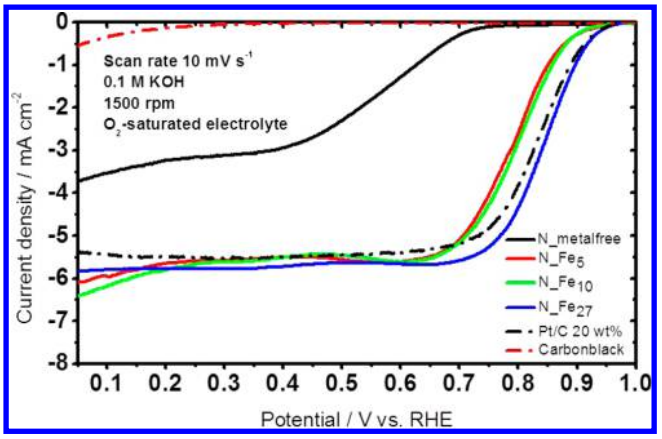

Figure 6. Linear sweep voltammetry (LSV) ORR plots in O_2-saturated 0.1 M KOH of different nominal metal content in comparison with metal-free N doped and Pt/C samples: (solid black) N-metalfree sample; (solid red) N_Fe$_5$; (solid green) N_Fe$_{10}$; (solid blue) N_Fe$_{27}$; (dashed black) Pt/C 20 wt %. The RDE experiments were carried out at room temperature, with a rotating speed of 1500 rpm, scan rate of 10 mV s^{-1}, non-noble-metal catalyst loading of 0.8 mg cm^{-2}, and Pt loading of 10 μg cm^{-2}.

230 mV anodic shift in ORR onset potential (0.63 to 0.86 V). Still, these hybrid catalysts trail pure Pt by about 20 mV in onset potential. The Fe-richest 27 wt % hybrid catalyst, however, outperforms pure Pt by about 20 mV with an onset potential of about 0.9 V. It is evident that the shift in E_{onset} between "N_metalfree" hybrid and "N_Fe$_x$" catalysts is larger by far than the activity improvements among the Fe hybrids: while the N_Fe$_5$ and N_Fe$_{10}$ samples showed similar onset potentials, the onset potential improved only by 40 mV by increasing the metal content from 10 wt % to 27 wt %.

The low diffusion-limited current for the metal-free catalyst evidences its low intrinsic activity but may also be affected by catalyst film quality and homogeneity. Diffusion-limited current values of the metal-containing hybrids are much closer to the hydrodynamic limit and the corresponding oxygen transport conditions. We thus conclude that the presence of metal in the synthesis of the final hybrid catalyst appears critical for levels of intrinsic ORR activity, rivaling pure Pt as well as hydrodynamically controlled diffusion patterns.

ORR Activity of Codoped Hybrid Catalysts. With 27 wt % determined to be the favorable nominal iron content, ORR tests were now performed for the codoped hybrid catalysts, including the metal-free and the respective 27 wt % metal-containing S/N, P/N, and B/N systems. ORR onset potentials (E_{onset}), half-wave potentials, and catalyst mass activities of these hybrid catalysts are summarized in Figure 7 and Table S5 (Supporting Information).

In order to avoid significant mass transport limitations, the electrode thickness for NNMCs should not exceed 100 μm. Therefore, for non-noble-metal catalyst materials volumetric activity is an important criterion. The corresponding volumetric ORR activities of the different catalysts are summarized in Table S5 (Supporting Information).

Voltammograms show that S/N_Fe$_{27}$ (E_{onset} = 0.93 V vs RHE) is a very active hybrid catalyst system, as its onset potential clearly exceeds that of Pt. It is the most active ORR catalyst of all hybrids considered here, while other codoped samples show onset potentials similar to that of the N-doped sample, N_Fe$_{27}$ (E_{onset} ≈ 0.86 V vs RHE).

dx.doi.org/10.1021/ja506553r | J. Am. Chem. Soc. 2014, 136, 14486−14497

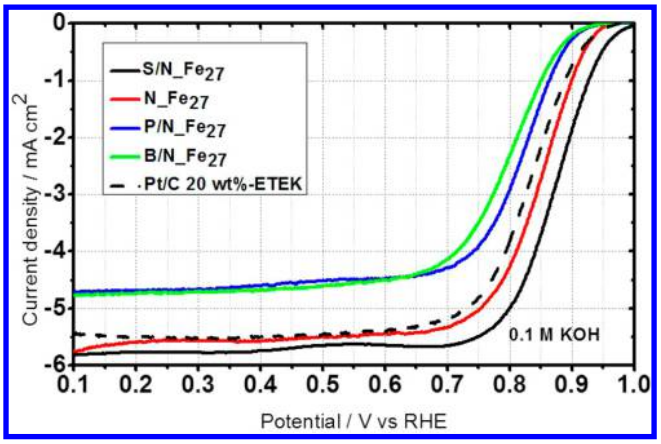

Figure 7. Linear sweep voltammetry (LSV) ORR plots in O_2-saturated 0.1 M KOH of different metal-free and metal-containing samples of different codoped systems in comparison with Pt/C samples: (solid red) N_Fe_{27} sample; (solid black) S/N_Fe_{27}; (solid blue) P/N_Fe_{27}; (solid green) B/N_Fe_{27}; (dashed black) Pt/C 20 wt %. The RDE experiments were carried out at room temperature, with a rotating speed of 1500 rpm, scan rate of 10 mV s^{-1}, non-noble-metal catalyst loading of 0.8 mg cm^{-2}, and Pt loading of 10 μg cm^{-2}.

Effect of Additional Leaching/Annealing. We have further performed ORR tests using the hybrid catalysts that underwent an additional second acid leaching and third annealing step (samples assigned as "N_Fe_x_2"). Mass activities of these hybrid catalysts under alkaline conditions are summarized in Figure 8A. Interestingly, the additional leaching/annealing steps resulted in doubling the mass activity values, thereby reaching the same onset potential with only half of the catalyst mass loading of 0.4 mg cm^{-2}. It is puzzling that for the "N_Fe_x_2" hybrid catalysts, unlike their singly leached analogues, the catalyst mass activities turned out to be very close to each other, being ~13 mA mg^{-1} for all metal contents (see Figure 8A).

Catalyst Durability. To probe the long-term stability of the hybrid catalysts, their mass activities were plotted before and after a severe two-step voltage cycling stability test (4500 and 9000 cycles) between 0.5 and 1.3 V in alkaline electrolyte (Figure 8A). At first sight, mass activity loss seems more dominant after 4500 cycles and remains relatively unchanged thereafter. Moreover, activity drops are more pronounced in N doped samples than in codoped heteroatomic systems. In addition, the stability decreased with increasing metal content from 5 to 27 wt % in alkaline electrolyte. Moreover, in order to explore the potential applicability of the novel metal-containing hybrids in acid PEMFCs, their ORR performance was evaluated in an acidic 0.1 M $HClO_4$ electrolyte (see Figure 8B). The activity trends in acid follow those observed in alkaline; however, the absolute mass activity values are drastically lower than those in acid medium. As Figure 8B further shows, the mass activity drop during voltage cycling is generally higher under acid than under alkaline conditions. It is worth noting that the codoped hybrids show clear stability advantages in both media, reflected in the much greater activity loss of N_Fe_{27} in comparison to the X/N_Fe_{27} (X = S, P, B) catalysts.

A Novel Active S/N_Fe_x ORR Hybrid Catalyst. The voltammetry and catalytic activity of the most active heteroatom codoped hybrid catalyst, S/N_Fe_{27}, were subsequently compared in more detail to those of a Pt reference catalyst in alkaline and acid electrolytes (see Figure 9). It is

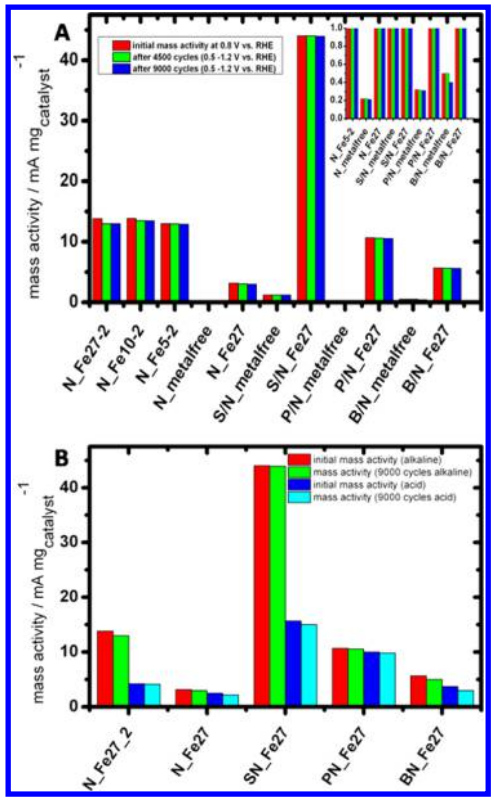

Figure 8. ORR mass activities of different singly doped and codoped samples at 0.8 V vs RHE in RDE before and after the stability test in N_2-saturated electrolyte; (A) in 0.1 M KOH (inset: mass activity of the metal-free samples before and after stability test); (B) in 0.1 M KOH and 0.1 M $HClO_4$ for metal-containing samples. The stability test was performed in N_2-saturated electrolyte with a scan rate of 50 mV s^{-1} in the potential range of 0.5−1.3 V vs RHE. ORR activity was measured after 4500 and 9000 cycles in O_2-saturated electrolyte.

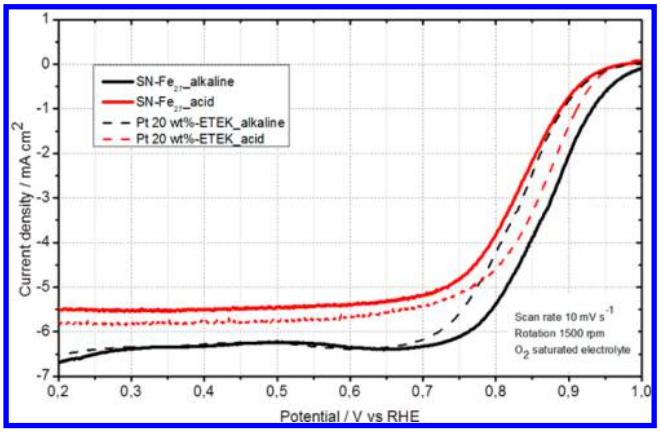

Figure 9. Rotating disk electrode (RDE) measurements of S/N_Fe_{27} catalyst in 0.1 M KOH (solid black) and 0.1 M $HClO_4$ (solid red), of Pt/C in alkali (dashed black), and of Pt/C in acid (dashed red).

worth noting that the onset potential of S/N_Fe_{27} in acid electrolyte was shifted cathodically by 0.03 V in comparison to Pt, which is an unprecedented ORR activity for non-noble-metal catalysts in $HClO_4$ environments.[13−18]

As expected, much higher activity was observed under alkaline conditions for the as-prepared S/N_Fe_{27} catalyst. Mukerjee et al. investigated the mechanistic origin, including surface media and coordination chemistry, which showed that

dx.doi.org/10.1021/ja506553r | J. Am. Chem. Soc. 2014, 136, 14486−14497

alkaline media facilitate the ORR on pyrolyzed non-noble-metal catalysts. New evidence shows that the involvement of surface-dependent outer-sphere electron transfer in the overall electrocatalytic process and surface nonspecificity are the fundamental reasons for the possibility of replacement of a platinum-based surface with a wide range of non-noble-metal surfaces as electrodes for ORR in alkaline media.[75,76]

Catalytic Oxygen Evolution Reaction on Nonprecious Heteroatom Codoped Hybrid Catalyst. Cyclic voltammetry (CV) was used to investigate the electrocatalytic activity and stability of the singly doped and codoped samples with the best ORR performance, N_Fe_{27} and S/N_Fe_{27}, with respect to the oxygen evolution reaction (OER) under alkaline pH conditions. This test checks for the potential applicability of these catalysts in alkaline water electrolysis. In Figure 10, the activities

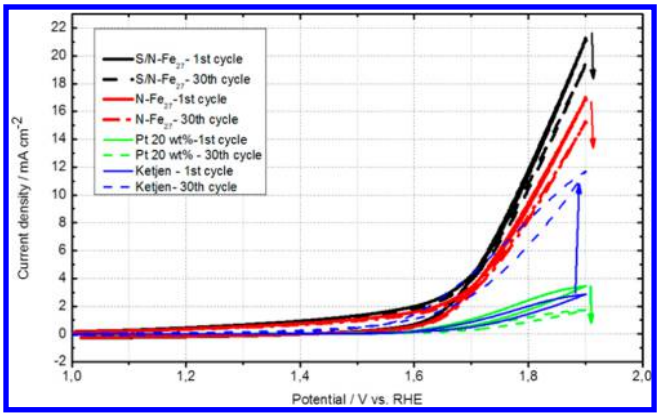

Figure 10. Electrocatalytic activity for OER of S/N_Fe_{27} (solid black), N_Fe_{27} (solid red), Pt/C 20 wt % (solid green), and Ketjenblack (solid blue) before stability tests. The corresponding plots with dashed lines are the OER activities after 30-cycle stability tests.

of the two catalysts are compared to those of pure carbon and pure Pt as references. Both IL-derived hybrid catalysts show catalytic performance significantly higher than that of the reference catalysts. It is noteworthy that the reported OER activity for these non-noble-metal catalysts is comparable to that of the most active NiO_x, FeO_x, and MnO_x OER catalysts. In particular, the activity of the codoped S/N_Fe_{27} sample is exceptional and outperforms that of the N_Fe_{27} catalyst. The overpotentials of both doped materials at 2 mA cm^{-2} were 180 mV lower than those for Pt/C and pure carbon catalysts.

Figure 10 shows that the catalytic activity advantage of the codoped over the singly doped hybrid catalyst ranges between 40 and 60 mV at 2 and 8 mA cm^{-2}, respectively, a trend that was observed for ORR activity as well. Cyclic voltammetry stability tests during OER catalysis between 1.0 and 2.0 V vs RHE were performed for 30 consecutive cycles. The recorded CVs after stability tests for as-synthesized catalysts and Pt are depicted in Figure 10 as dashed lines. This shows a general decrease in OER activity; however, the stability advantage of the heteroatom system is obvious. Accordingly, for N_Fe_{27} and S/N_Fe_{27}, the overpotential changes by only 10 mV after stability cycling at 8 mA cm^{-2}. Differential electrochemical mass spectrometry studies of the reaction products during the OER (see Figure S11, Supporting Information) show that the strongly graphitized heteroatom doped catalyst shows a remarkable stability in comparison to the Ketjenblack regarding carbon corrosion and CO_2 formation. While pure Ketjenblack massively corroded and evolved CO_2 above ~ 2.1 V vs RHE, the heteroatom doped catalysts remained stable under these conditions, resulting in high Faradaic selectivity for molecular oxygen.

CORRELATING STRUCTURE, COMPOSITION, AND ELECTROCHEMICAL ACTIVITY FOR HETEROATOM DOPED HYBRIDS

Empirical relationships between functional catalytic activity and structure, composition, and morphology help identify and distinguish between more and less significant factors controlling catalytic performance. On the basis of the results illustrated in Figures 6 and 8, we unambiguously conclude that the presence of Fe during synthesis significantly enhanced the ORR activity of the hybrid materials. This is consistent with most previous studies on nonprecious ORR catalysts. In this work, in all hybrid catalysts except one, Fe was observed in the form of crystalline iron carbide, which indeed was previously suspected to be a catalytically active phase for ORR. However, exceptionally, the "P/N_Fe_{27}"—with a 0.25 V anodic ORR onset potential shift in comparison to its P/N_metalfree reference and an absolute ORR activity of P/N_Fe_{27} similar to that of the N_Fe_{27} and B/N_Fe_{27} hybrids—did not show any traces of crystalline Fe carbide. This may suggest that the presence of P prevents the formation of crystalline Fe carbides and that Fe is present in some other X-ray amorphous form, possibly amorphous Fe phosphide phases. On the basis of these observations, there are two possible explanations for the activity trends in the X/N_Fe_{27} hybrid systems: (i) iron carbide, which has been reported as the active moiety for ORR,[77] does not play the role of the dominant active phase in as-synthesized samples in this work; (ii) the catalytically active moieties in P/N_Fe_{27} are different in chemical nature in comparison to the other hybrid catalysts. Unsuccessful detection of iron species using XPS makes it difficult to draw a clearer picture about the iron environment in the samples; however, it prompts the conclusion that there are only a few Fe centers in the near-surface region. It is worth noting that the correlation of the surface area and the heteroatom content with ORR mass activity appears as a much more straightforward and promising pathway toward insight into the activity-controlling parameters. Figure 11 depicts how the experimental catalyst mass activity changes for different samples with regard to their BET surface area and heteroatom content (nitrogen and second heteroatom (S, P and B)). Obviously, achieving higher BET surface areas results in a more active sample, as all the samples with high mass activity have a BET surface area of higher than 800 m^2 $g_{catalyst}^{-1}$ (Figure 11A). However, the most active catalyst (S/N_Fe_{27}) does not have the highest BET surface area. Interestingly, the activities of the family of N_Fe_x-2 samples with different iron loadings follow their relatively identical surface areas. Moreover, Figure 11B shows that there is no clear correlation between nitrogen content and activity of the final materials. It is worth noting that the content of second heteroatom in S/N and B/N codoped materials shows an inverse trend with activity. The addition of metal results in reducing the second heteroatom in the samples, which forms a more active catalyst. This observation is not the case for the P/N codoped catalyst, meaning that the catalyst with higher P content has greater activity.

Therefore, we conclude that the final activity of the as-synthesized catalysts is influenced by multiple variable factors, including BET surface area, nitrogen/second heteroatom content, and the iron carbide moieties. Accordingly, a highly

dx.doi.org/10.1021/ja506553r | J. Am. Chem. Soc. 2014, 136, 14486−14497

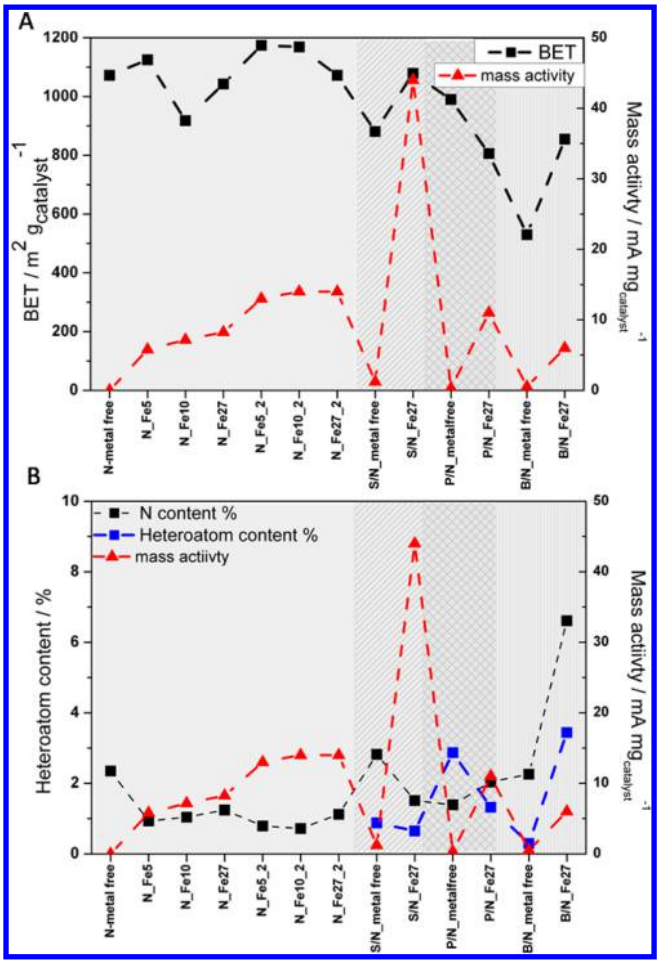

Figure 11. (A) BET surface area (m^2 g^{-1}) (black dashed) and (B) nitrogen (black dashed) and second heteroatom (blue dashed) contents of various heteroatom doped hybrid catalysts plotted with their mass activity (mA mg^{-1} (@ 0.8 V) (red dashed).

interesting conclusion can yet be made when the chemical state of the different heteroatoms within the carbon hybrids is taken into account. As discussed previously regarding the XPS spectra of the different materials, the two types of heteroatoms (S and N) in the most ORR active catalyst, S/N_Fe_{27}, are most likely to be incorporated into the carbon backbone separately from each other. For the codoping with B and N or P and N, it is more likely that direct chemical bonds between the two dopants are dominant. Especially, for B/N codoping this might result in a mutual compensation of the doping effects of electron-poor boron and electron-rich nitrogen. In contrast, in the highly active S/N_Fe_{27} material, no mutual compensation of doping effects can occur, due to the different chemical environments.

CONCLUSION

We have successfully developed and utilized synthetic protocols for a controlled chemical heteroatom doping of high-surface-area carbon using ILs in order to prepare novel and catalytically highly active carbon hybrid materials with tunable heteroatom doping profiles (N, S/N, P/N, and B/N). Thereby, we explored the hypothesis whether heteroatom codoping can give rise to enhanced synergetic catalytic performance. The differently doped systems were compared systematically with respect to their ORR and OER activity. We have established trends in ORR activity among the codoped hybrid systems and have identified the S/N codoped material synthesized using a ferric chloride mediator (S/N_Fe_{27}) as the most active ORR catalyst under both alkaline and acid conditions, outperforming monodoped N_Fe_x. This clearly emphasizes the beneficial effect of dual doping. Accordingly, the activity of S/N_Fe_{27} in acid solution meets that of Pt. In alkaline solution, the S/N material outperforms Fe−N−C materials reported earlier.

Our findings confirm that the introduction of Fe metal in the synthetic protocol is a critical requirement for high ORR activity. This did yet not go along with proving the involvement of Fe in the catalytically active phase. In fact, the observed ORR activity was essentially independent of the absolute Fe content, and the Fe content was below the detection limit in near-surface regions of the hybrid materials according to XPS measurements. However, metal was present in most hybrids according to diffraction patterns as crystalline iron carbide. However, no metal was detected in the P/N codoped catalyst, which is most likely to rule out crystalline Fe carbides as the only active phase.

Our findings strengthen the idea that the catalytically active functional site is strongly influenced by the doping heteroatoms and that the ORR activity of the materials is controlled by the nature and especially the chemical position of the heteroatoms with respect to each other, while iron may be present in the catalytically active site or serve as a mediator to generate the active site during the synthetic process. In this case, we assume that independent doping of N and S into a carbonaceous structure, which is confirmed by XPS data, can create distinct characteristic electronic distribution and structure in the final catalyst for the S/N_Fe_{27} sample in comparison to the other codoped samples (P/N and B/N).

This study translates previous insight into ORR active N-doped materials to new heteroatoms by providing the first hints of a synergetic catalytic effect of heteroatom pairs. Thereby, this study opens up new synthetic control of parameters affecting the final structure and catalyst performance. Additionally, it also points to unexplored avenues toward new multiply heteroatom doped nonprecious ORR catalysts. The rational design and integration of two or more heteroatoms may lead to a new family of catalyst materials with tunable catalytic properties.

ASSOCIATED CONTENT

Supporting Information

This material is available free of charge via the Internet at http://pubs.acs.org.

AUTHOR INFORMATION

Corresponding Authors

*E-mail for J.P.P.: jens.p.paraknowitsch@tu-berlin.de.
*E-mail for P.S.: pstrasser@tu-berlin.de.

Notes

The authors declare no competing financial interest.

ACKNOWLEDGMENTS

N.R.S would like to thank unicat (unifying concept in catalysis) and BIG-NSE (Berlin international Graduate School of Natural Sciences and Engineering) for financial supports. This work was partially supported by the Deutsche Forschungsgemeinschaft (DFG)under grant STR 596/4-1.

REFERENCES

(1) Jasinski, R. *Nature* **1964**, *201*, 1212.
(2) Chen, Z.; Higgins, D.; Yu, A.; Zhang, L.; Zhang, J. *Energy Environ. Sci.* **2011**, *4*, 3167.
(3) Ferrandon, M.; Kropf, A. J.; Myers, D. J.; Artyushkova, K.; Kramm, U.; Bogdanoff, P.; Wu, G.; Johnston, C. M.; Zelenay, P. *J. Phys. Chem. C* **2012**, *116*, 16001.
(4) Lei, Z.; Jiujun, Z.; Wilkinson, D. P.; Haijiang, W. *J. Power Sources* **2006**, *156*, 171.
(5) Rabis.; et al. *ACS Catal.* **2014**, *2*, 864.
(6) Wu; Zelenay. *Acc. Chem. Res.* **2013**, *46*, 1878.
(7) Dodelet, J. P.; et al. *Science* **2009**, *324*, 71.
(8) Dodelet, J. P.; et al. In *N4-Macrocyclic Metal Complexes*; Springer: New York, 2006; p 83.
(9) Subramarian, N. P.; et al. *J. Power Sources* **2006**, *157*, 56.
(10) Jaouen, F.; Dodelet, J. P. *J. Phys. Chem. C* **2007**, *111*, 5963.
(11) Jaouen, F.; Charreteur, F; Dodelet, J. P. *J. Electrochem. Soc.* **2006**, *153*, A689.
(12) Serov, A.; Robson, M. H.; Smolnik, M.; Atanassov, P. *Electrochim. Acta* **2012**, *80*, 213.
(13) Ozaki, J.-i.; Anahara, T.; Kimura, N.; Oya, A. *Carbon* **2006**, *44*, 3358.
(14) Shuangyin Wang, E. I.; Roy, A.; Xue, Y.; Yu, D.; Liming, D. *Angew. Chem., Int. Ed.* **2011**, *50*, 11756.
(15) Sheng, Z.-H.; Gao, H.-L.; Bao, W.-J.; Wang, F.-B.; Xia, X.-H. *J. Mater. Chem.* **2012**, *22*, 390.
(16) Yang, Z.; Yao, Z.; Li, G.; Fang, G.; Nie, H.; Liu, Z.; Zhou, X.; Chen, X. a.; Huang, S. *ACS Nano* **2012**, *6*, 205.
(17) Wu, J.; Yang, Z.; Li, X.; Sun, Q.; Jin, C.; Strasser, P.; Yang, R. *J. Mater. Chem. A* **2013**, *1*, 9889.
(18) Paraknowitsch, J. P.; Thomas, A. *Energy Environ. Sci.* **2013**, *6*, 2839.
(19) Shao, Y. Y.; Y., G. P.; Wang, J. J.; Gao, Y. Z.; Shi, P. F. *J. Power Sources* **2006**, *161*, 47.
(20) Shao-Horn, Y.; S., W. C.; Chen, S.; Ferreira, P. J.; Holby, E. F.; Morgan, D. *Top. Catal.* **2007**, *46*, 285.
(21) Walden, P. *Bull. Acad. Imp. Sci. St.-Petersbourg* **1914**, *8*, 405.
(22) Earle, M. J.; Seddon, K. R. *Pure Appl. Chem.* **2000**, *72*, 1391.
(23) Swatloski, R. P.; Spear, S. K.; Holbrey, J. D.; Rogers, R. D. *J. Am. Chem. Soc.* **2002**, *124*, 4974.
(24) Hallett, J. P.; Welton, T. *Chem. Rev.* **2011**, *111*, 3508.
(25) Welton, T. *Chem. Rev.* **1999**, *99*, 2071.
(26) Parvulescu, V. I.; Hardacre, C. *Chem. Rev.* **2007**, *107*, 2615.
(27) Sheldon, R. *Chem. Commun.* **2001**, 2399.
(28) Wasserscheid, P.; Keim, W. *Angew. Chem., Int. Ed.* **2000**, *39*, 3772.
(29) Welton, T. *Coord. Chem. Rev.* **2004**, *248*, 2459.
(30) Fellinger, T.-P.; Thomas, A.; Yuan, J.; Antonietti, M. *Adv. Mater.* **2013**, *25*, 5838.
(31) Paraknowitsch, J. P.; Thomas, A. *Macromol. Chem. Phys.* **2012**, *213*, 1132.
(32) Antonietti, M.; Kuang, D. B.; Smarsly, B.; Yong, Z. *Angew. Chem., Int. Ed.* **2004**, *43*, 4988.
(33) Ma, Z.; Yu, J. H.; Dai, S. *Adv. Mater.* **2010**, *22*, 261.
(34) Parnham, E. R.; Morris, R. E. *Acc. Chem. Res.* **2007**, *40*, 1005.
(35) Carriazo, D.; Concepcion Serrano, M.; Concepcion Gutierrez, M.; Luisa Ferrer, M.; del Monte, F. *Chem. Soc. Rev.* **2012**, *41*, 4996.
(36) Abbott, A. P.; Capper, G.; Davies, D. L.; Rasheed, R. K.; Tambyrajah, V. *Chem. Commun.* **2003**, 70.
(37) Lee, J. S.; Wang, X. Q.; Luo, H. M.; Baker, G. A.; Dai, S. *J. Am. Chem. Soc.* **2009**, *131*, 4596.
(38) Lee, J. S.; Wang, X. Q.; Luo, H. M.; Dai, S. *Adv. Mater.* **2010**, *22*, 1004.
(39) Paraknowitsch, J. P.; Thomas, A.; Antonietti, M. *J. Mater. Chem.* **2010**, *20*, 6746.
(40) Paraknowitsch, J. P.; Zhang, J.; Su, D. S.; Thomas, A.; Antonietti, M. *Adv. Mater.* **2010**, *22*, 87.
(41) Wooster, T. J.; Johanson, K. M.; Fraser, K. J.; MacFarlane, D. R.; Scott, J. L. *Green Chem.* **2006**, *8*, 691.
(42) Fellinger, T.-P.; Su, D. S.; Engenhorst, M.; Gautam, D.; Schloegl, R.; Antonietti, M. *J. Mater. Chem.* **2012**, *22*, 23996.
(43) Fulvio, P. F.; Lee, J. S.; Mayes, R. T.; Wang, X.; Mahurin, S. M.; Dai, S. *Phys. Chem. Chem. Phys.* **2011**, *13*, 13486.
(44) Paraknowitsch, J. P.; Wienert, B.; Zhang, Y.; Thomas, A. *Chem. Eur. J.* **2012**, *18*, 15416.
(45) Fechler, N.; Fellinger, T.-P.; Antonietti, M. *J. Mater. Chem. A* **2013**, *1*, 14097.
(46) Paraknowitsch, J. P.; Zhang, Y.; Wienert, B.; Thomas, A. *Chem. Commun.* **2013**, *49*, 1208.
(47) Hasche, F.; Fellinger, T.-P.; Oezaslan, M.; Paraknowitsch, J. P.; Antonietti, M.; Strasser, P. *ChemCatChem* **2012**, *4*, 479.
(48) Yang, W.; Fellinger, T. P.; Antonietti, M. *J. Am. Chem. Soc.* **2011**, *133*, 206.
(49) Fellinger, T.-P.; Hasche, F.; Strasser, P.; Antonietti, M. *J. Am. Chem. Soc.* **2012**, *134*, 4072.
(50) Shao, Y. Y.; Sui, J. H.; Yin, G. P.; Gao, Y. Z. *Appl. Catal. B-Environ.* **2008**, *79*, 89.
(51) Wang, S.; Iyyamperumal, E.; Roy, A.; Xue, Y.; Yu, D.; Dai, L. *Angew. Chem., Int. Ed.* **2011**, *50*, 11756.
(52) Yang, L.; Jiang, S.; Zhao, Y.; Zhu, L.; Chen, S.; Wang, X.; Wu, Q.; Ma, J.; Ma, Y.; Hu, Z. *Angew. Chem., Int. Ed.* **2011**, *50*, 7132.
(53) Yang, Z.; Yao, Z.; Li, G.; Fang, G.; Nie, H.; Liu, Z.; Zhou, X.; Chen, X. a.; Huang, S. *ACS Nano* **2011**, *6*, 205.
(54) Wu, J.; Yang, Z.; Li, X.; Sun, Q.; Jin, C.; Strasser, P.; Yang, R. *J. Mater. Chem. A* **2013**, *1*, 9889.
(55) Tuaev, X.; Paraknowitsch, J. P.; Illgen, R.; Thomas, A.; Strasser, P. *Phys. Chem. Chem. Phys.* **2012**, *14*, 6444.
(56) Thommes, M. In *Nanoporous Materials: Science and Engineering*; Lu, G. Q., Zhao, X. S., Eds.; Imperial College Press: London, 2004.
(57) Brunauer, S.; Emmett, P. H.; Teller, E. *J. Am. Chem. Soc.* **1938**, *60*, 309.
(58) Gardin, A. I. *Kristallografiya* **1962**, *7*, 854.
(59) The International Centre for Diffraction Data: 2009.
(60) Moulder, J. F.; Stickle, W. F.; Sobol, P. E.; Bomben, K. D. In *Handbook of X-ray Photoelectron Spectroscopy*; Chastain, J., Ed.; Perkin Elmer: Eden Prairie, MN, 1992.
(61) Choi, C. H.; Park, S. H.; Woo, S. I. *Green Chem.* **2011**, *13*, 406.
(62) Silien, C.; Buck, M.; Goretzki, G.; Lahaye, D.; Champness, N. R.; Weidner, T.; Zharnikov, M. *Langmuir* **2009**, *25*, 959.
(63) Panzner, G.; Diekmann, W. *Surf. Sci.* **1985**, *160*, 253.
(64) Pietrzak, R.; Wachowska, H.; Nowicki, P. *Energy Fuels* **2006**, *20*, 1275.
(65) Burg, P.; Fydrych, P.; Cagniant, D.; Nanse, G.; Bimer, J.; Jankowska, A. *Carbon* **2002**, *40*, 1521.
(66) Huang, M. C.; Teng, H. S. *Carbon* **2003**, *41*, 951.
(67) National Institute of Standards and Technology, Gaithersburg, MD.
(68) Lindberg, B. J.; Hamrin, K.; Johansson, G.; Gelius, U.; Fahlman, A.; Nordling, C.; Siegbahn, K. *Phys. Scr.* **1970**, *1*, 286.
(69) Liu, G.; Niu, P.; Sun, C. H.; Smith, S. C.; Chen, Z. G.; Lu, G. Q.; Cheng, H. M. *J. Am. Chem. Soc.* **2010**, *132*, 11642.
(70) Gonçalves, A. M.; Njel, C.; Mathieu, C.; Aureau, D.; Etcheberry, A. *Thin Solid Films* **2013**, *538*, 21.
(71) CNRS: lasurface.com.
(72) Allcock, H. R.; Steely, L. B.; Kim, S. H.; Kim, J. H.; Kang, B.-K. *Langmuir* **2007**, *23*, 8103.
(73) Jacobsohn, L. G.; Schulze, R. K.; Maia da Costa, M. E. H.; Nastasi, M. *Surf. Sci.* **2004**, *572*, 418.
(74) Guimon, C.; Gonbeau, D.; Pfister-Guillouzo, G.; Dugne, O.; Guette, A.; Naslain, R.; Lahaye, M. *Surf. Interface Anal.* **1990**, *16*, 440.
(75) Ramaswamy, N.; Mukerjee, S. *Adv. Phys. Chem.* **2012**, *2012*, 17.
(76) Ramaswamy, N.; Tylus, U.; Jia, Q.; Mukerjee, S. *J. Am. Chem. Soc.* **2013**, *135*, 15443.
(77) Lee, J.-S.; Park, G. S.; Kim, S. T.; Liu, M.; Cho, J. *Angew. Chem., Int. Ed.* **2013**, *52*, 1026.